Detection and Classification of Hyper-Spectral Edges

Harro Stokman and Theo Gevers
ISIS, University of Amsterdam, Kruislaan 403
1098 SJ Amsterdam, The Netherlands
{stokman, gevers}@wins.uva.nl

Abstract

Intensity-based edge detectors cannot distinguish whether an edge is caused by material changes, shadows, surface orientation changes or by highlights. Therefore, our aim is to classify the physical cause of an edge using hyper-spectra obtained by a spectrograph. Methods are presented to detect edges in hyperspectral images. In theory, the effect of varying imaging conditions is analyzed for "raw" hyper-spectra, for normalized hyper-spectra, and for hue computed from hyper-spectra. From this analysis, an edge classifier is derived which distinguishes hyper-spectral edges into the following types: (1) a shadow or geometry edge, (2) a highlight edge, (3) a material edge.

1 Introduction

Edge information from an image can be used to measure or recognize objects in images. Edges correspond to significant changes in the image, ideally at the boundary between two different regions. However, false edges are often detected, and (parts of) important edges are missing. Thus, after edge detection there remains the problem of obtaining meaningful information about object boundaries using edges. We therefore believe that the classification of edges in for instance shadow edge, geometry edge, highlight edge or material edge, is useful. Intensity-based edge detectors cannot distinguish the physical cause of an edge. In this paper, hyper-spectra are therefore used to classify the edges.

Physics-based segmentation methods have been studied for RGB images. Klinker et al. [5] and Bajscy et al. [1] retrieve "dog-leg" planar clusters in RGB space. The segmentation results are independent of different imaging conditions caused by the object geometry, illumination and by highlights. Healey [4] proposed a physics-based method to segment images on the basis of normalized color. In this paper, methods are presented for hyper-spectral color space transforms. The effect of varying imaging conditions is then analyzed for raw hyper-spectra, for normalized hyper-spectra, and for the hue computed from hyper-spectra.

A number of well established techniques for edge detection in ordinary (one-band) images are available [2] for example. There are various ways to combine the edge gradients computed from the different color bands. In this paper, we will use the principled method proposed by diZenzo [7] to combine the gradients of the hyper-spectral images. Gevers presented in [3] an edge classification scheme which operated on edge maps from $c_1c_2c_3$

and $l_1 l_2 l_3$ color spaces. The models are derived from RGB data. In this paper, we extend the edge detection and classification scheme to operate on color models derived from hyper-spectra. Given the hyper-spectral gradients, we then employ the physics-based edge classification scheme to distinguish edges into the following types: (1) a shadow or geometry edge, (2) a highlight edge, (3) a material edge.

The paper is organized as follows. In Section 2, the dichromatic reflection model is discussed. In Section 3, methods are presented for hyper-spectral color space transforms and to detect edges in hyperspectral images. The edge classifier is given in Section 4. Experiments are discussed in Section 5.

2 Dichromatic Reflection Model

Consider an image of an infinitesimal surface patch. Using N narrow-band filters with spectral sensitivities given by $f_1(\lambda)...f_N(\lambda)$ to obtain an image of the surface patch illuminated by a spectral power distribution of the incident light denoted by $e(\lambda)$, the measured sensor values are given according to Shafer [6] as:

$$C_n = m_b(\vec{n}, \vec{s}) \int_\lambda f_n(\lambda) e(\lambda) c_b(\lambda) d\lambda + m_s(\vec{n}, \vec{s}, \vec{v}) \int_\lambda f_n(\lambda) e(\lambda) c_s(\lambda) d\lambda \tag{1}$$

for C_n giving the nth sensor response. Further, $c_b(\lambda)$ and $c_s(\lambda)$ are the albedo and Fresnel reflectance respectively. λ denotes the wavelength, $\vec{n}$ is the surface patch normal, $\vec{s}$ is the direction of the illumination source, and $\vec{v}$ is the direction of the viewer. Geometric terms m_b and m_s denote the geometric dependencies on the body and surface reflection respectively and their range is $0 \leq m_b(\vec{n}, \vec{s}) + m_s(\vec{n}, \vec{s}, \vec{v}) \leq 1$. A matte object is described by the body reflection, a shiny object by both the body and surface reflection. The neutral interface reflection model assumes that the Fresnel reflectance has a constant value over for all wavelengths in the visible spectrum. The surface reflection term of Eq. 1 is then written as $m_s(\vec{n}, \vec{s}, \vec{v}) c_s \int_\lambda f_n(\lambda) e(\lambda) d\lambda$. The dichromatic reflection model is valid for inhomogeneous dielectric materials and will be used to study and analyze the transformed color spaces derived from hyper-spectra.

3 Photometric Invariance of Color Spaces Derived from Hyper-Spectra

3.1 Photometric Invariance of Normalized Hyper-Spectra

Given a hyper-spectrum of N samples, the normalized hyper-spectrum is computed as

$$c_n = \frac{C_n}{C_1 + \cdots + C_N} \tag{2}$$

For a matte object, the normalized hyper-spectrum is invariant to the geometry of the object. If the terms $m_b(\vec{n}, \vec{s})$ and $\int_\lambda f_n(\lambda) e(\lambda) c_b(\lambda) d\lambda$ of Eq. 1 are abbreviated to m_b and k_n respectively, then the substitution of Eq. 1 in Eq. 2 gives

$$c_n = \frac{m_b k_n}{m_b(k_1 + \cdots + k_N)} = \frac{k_n}{k_1 + \cdots + k_N} \tag{3}$$

independent of $m_b(\vec{n}, \vec{s})$. In other words, normalized hyper-spectrum is invariant to shading and the shape of the object.

3.2 Calculation and Photometric Invariance of Hyper-Spectral Hue

Calculations Involving Hue The hue describes the tint of a color, e.g. red, green or blue. Hue orders colors in a circular mode. As a consequence, calculations involving hue require special care. If a number of hues are to be added, where w_k corresponds to a weighting factor for the kth hue H_k, we propose to decompose first the hue angles in a horizontal and vertical component, and then to multiply these components with the weights. The hue should then be taken as the angle between the summed horizontal and vertical component. More specific:

$$g(\{w_1, \cdots, w_N\}, \{H_1, \cdots, H_N\}) = \arctan\left(\frac{\sum_i w_i \cos(H_i)}{\sum_i w_i \sin(H_i)}\right) \tag{4}$$

where weights w_k of the set of weights $\{w_1, \cdots, w_N\}$ corresponds to the hue H_k of the set of hues $\{H_1, \cdots, H_N\}$.

To compute the difference between two hues H_1 and H_2, we propose that the hue angles are first decomposed in a horizontal and vertical component, and to take the Euclidean distance between these components as the hue difference. More specific:

$$\text{diff}(H_1, H_2) = [(\cos(H_1) - \cos(H_2))^2 + (\sin(H_1) - \sin(H_2))^2]^{1/2} \tag{5}$$

which gives a difference diff$(H_1, H_2) \in [0, 2]$ between H_1 and H_2.

To derive the derivative of a hue image, we proceed as follows. Consider the first derivative of the Gaussian $G'(x, \sigma)$ where x is a one-dimensional hue image and σ the spread of the Gaussian. Split $G'(x, \sigma)$ at the zero-crossing. Compute the weighted hue sum for the two components using the weights of the split $G'(x, \sigma)$, and take the hue difference of the two results as the derivative. More specific:

$$\begin{aligned} \nabla_H = \ \text{diff}(H_1, H_2) \quad \text{where} \quad & H_1 = g(\{w_1, \cdots, w_{N/2}\}, \{H_1, \cdots, H_{N/2}\}) \\ & H_2 = g(\{w_{N/2}, \cdots, w_N\}, \{H_{N/2}, \cdots, H_N\}) \\ \text{and} \quad & \{w_1, \cdots, w_{N/2}\} = G'(x, \sigma); x \in (-\infty, 0) \\ & \{w_{N/2}, \cdots, w_N\} = G'(x, \sigma); x \in (0, +\infty) \end{aligned} \tag{6}$$

where $g()$ is defined by Eq. 4.

Obtaining Equal-Energy Illumination Consider the reflectance of a matte, white reference with constant spectral response, $c_b(\lambda)$ = constant = 1. Assume that the surface normal is equal to the illumination direction, thus $m_b(\vec{n}, \vec{s}) = 1$. As no specularities occur, the measured sensor values are, according to Eq. 1:

$$C_n = \int_\lambda f_n(\lambda) e(\lambda) d\lambda \tag{7}$$

for C_n giving the nth sensor response for the white reference sample. This way, the spectral transmittance of the illuminant is measured. Next, an image is captured of an arbitrary scene, and is divided by the previously obtained recording of the illuminant:

$$C_n = \frac{m_b(\vec{n},\vec{s}) \int_\lambda f_n(\lambda)e(\lambda)c_b(\lambda)d\lambda}{\int_\lambda f_n(\lambda)e(\lambda)d\lambda} + \frac{m_s(\vec{n},\vec{s},\vec{v})c_s \int_\lambda f_n(\lambda)e(\lambda)d\lambda}{\int_\lambda f_n(\lambda)e(\lambda)d\lambda} \tag{8}$$

for C_n giving the nth sensor response. Now assume that the filter $f_n(\lambda)$ is a narrow band filter modeled as a unit impulse that is shifted over n wavelengths: The transmission at $\lambda_n = \delta$ and zero elsewhere. This allows Eq. 8 to be written as:

$$C_n = \frac{m_b(\vec{n},\vec{s}) f_n(\lambda)e(\lambda)c_b(\lambda)}{f_n(\lambda)e(\lambda)} + \frac{m_s(\vec{n},\vec{s},\vec{v})c_s f_n(\lambda)e(\lambda)}{f_n(\lambda)e(\lambda)} \tag{9}$$

and thus

$$C_n = m_b(\vec{n},\vec{s})c_b(\lambda) + m_s(\vec{n},\vec{s},\vec{v})c_s \tag{10}$$

implying that, under the assumption of a unit impulse band filter, the imagery can be made independent of the illuminant, if the original image is divided by the spectral transmittance of the illuminant.

Removal of the Saturation from the Hyper-Spectrum Saturation encodes how much the color of the illuminant (e.g. white) is mixed with the pure hue (e.g. red). Removal of the saturation from a spectrum is a two-step process: First, the spectrum is made independent of the illuminant, as described in the previous paragraph. Second, under equal-energy illumination, desaturating the spectrum consists of the subtraction of the maximum quantity of equal-energy of the spectrum. More specific, we propose that all spectral samples from a spectrum are transformed as:

$$c_i = C_i - \min\{C_1, \cdots, C_N\} \tag{11}$$

As a result, the transformed spectrum is invariant to highlights: If $m_{b,n}(\vec{n},\vec{s})c_b(\lambda)+$ $m_s(\vec{n},\vec{s},\vec{v})c_s$ of Eq. 10 is abbreviated to $m_b k_n + m_s c_s$, and let

$$m_b k_{min} + m_s c_s = \min\{m_b k_1 + m_s c_s, \cdots, m_b c_N + m_s c_s\} \tag{12}$$

The substitution of Eq. 10 in Eq. 11 now gives

$$c_n = (m_b k_n + m_s c_s) - (m_b k_{\min} + m_s c_s) = m_b(k_n - k_{\min}) \tag{13}$$

Since Eq. 13 is independent of $m_s(\vec{n},\vec{s},\vec{v})$, it is proven that, under the condition of equal-energy illumination, the desaturated spectrum is independent of highlights.

Hue Calculation from the Hyper-Spectrum After pre-processing of the spectrum according to Eq. 8 and Eq. 11, the hue can be calculated directly from the hyper-spectrum. Each spectral sample C_k is assigned a hue. The intensity of the sample is taken as the weight of the assigned hue. The hue angle is then computed by weighted hue addition using Eq. 4. More specific, we propose to compute the hue from the hyper-spectrum as:

$$H(C_1, \cdots, C_N) = g(\{C_1, \cdots, C_N\}, \{f(1), \cdots, f(N)\}) \text{ where } f(i) = \frac{(i-1)2\Pi}{N} \tag{14}$$

where function $g()$ has been specified in Eq. 4, and the function $f(i)$ assigns a hue to the ith of N spectral samples. Since the input of the function is the desaturated spectrum, the hue is invariant to highlights. Moreover, the hue is also independent of shadows and geometry. To prove this, the transformed spectrum of Eq. 13 is substituted in Eq. 14:

$$\begin{aligned} H(C_1, ..., C_N) &= \arctan\left(\frac{(m_b k_1 - m_b k_{min})\cos(f(1)) + ... + (m_b k_N - m_b k_{min})\cos(f(N))}{(m_b k_1 - m_b k_{min})\sin(f(1)) + ... + (m_b k_N - m_b k_{\min})\sin(f(N))}\right) \\ &= \arctan\left(\frac{(k_1 - k_{\min})\cos(f(1)) + ... + (k_N - k_{\min})\cos(f(N)}{(k_1 - k_{\min})\sin(f(1)) + ... + (k_N - k_{\min})\sin(f(N)}\right) \end{aligned} \tag{15}$$

independent of $m_b(\vec{n}, \vec{s})$. Hence, hue is invariant to the geometry of the object and shadows.

4 Reflectance Based Edge Classification

Edges are detected by taking the first derivative of a Gaussian from the "raw" and normalized hyper-spectra. The derivative of the hue is computed according to Eq. 6. The principled method proposed by diZenzo [7] is used to combine the gradients of the hyper-spectral and normalized hyper-spectral images. In the previous sections, the effect of varying imaging circumstances was analyzed in theory using the dichromatic reflection model for a hyper-spectrum, a normalized hyper-spectrum, and for the hue computed from the hyper-spectrum. As a result of this varying dependence on imaging conditions, the gradients $\nabla_{raw}, \nabla_{norm}, \nabla_{hue}$ computed from the raw hyper-spectra, normalized hyper-spectra, and hues respectively, are invariant or sensitive to these imaging conditions. The taxonomy is given in Table 1. Based on this gradient taxonomy, we propose a color edge classifier that distinguishes edges of the following types: (1) shadow or geometry edges, (2) highlight edges, (3) material edges, as follows:

if $\nabla_{raw} > t_{raw}$ **and** $\nabla_{norm} \leq \nabla_{norm}$
then classify ∇_{raw} as shadow or geometry edge
else **if** $\nabla_{raw} > t_{raw}$ **and** $\nabla_{hue} \leq t_{hue}$
then classify ∇_{norm} as highlight edge
else **if** $\nabla_{hue} > t_{hue}$
then classify ∇_{hue} as material edge

For each edge map $\nabla_{raw}, \nabla_{norm}, \nabla_{hue}$, edge pixels are identified by the selection of gradient magnitude thresholds $t_{raw}, t_{norm}, t_{hue}$ respectively. These threshold values can be based on the noise level in the image, or can be set manually.

5 Experiments

In Fig. 1a, a red and a yellow wooden block are shown. The red block is oriented such, that one side is shaded. A region is marked in white from which a hyper-spectral line-scan image is taken. Hyperspectral images are obtained using the Imspector V7 spectograph, Jain CV-M300 camera and Matrox Corona Framegrabber, under Philips Practitone A60 Daylight illumination. The hyper-spectral image is shown in Fig. 1b. The hyper-spectral image of 760 x 580 pixels is filtered along the spectral axis with a uniform filter of size 9,

	geometry/shadow	highlight	material
∇_{raw}	+	+	+
∇_{norm}	-	+	+
∇_{hue}	-	-	+

Table 1: *Taxonomy of color edges, - denotes invariant and + denotes sensitivity. The gradient of raw hyper-spectra ∇_{raw} is influenced by the geometry, shadows, object reflectance and highlights. The gradient of normalized hyper-spectra ∇_{norm} is independent of geometry and shadows, but is influenced by highlights and object reflectance. The gradient of hue ∇_{hue} is only influenced by a change in object reflectance, which is caused by material transitions.*

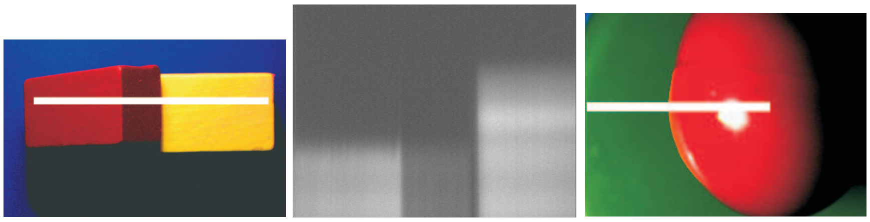

(a) (b) (c)

Figure 1: *a: Red and yellow wooden block. One side of the red block is shaded A region is marked in white from which a hyper-spectral line-scan image is taken, which is shown in b. Here, the top of the vertical axis corresponds to 400 nm, the bottom line corresponds to 700 nm. The horizontal axis represent spatial information. The gray values represent the reflectance of the objects. The image can be divided in three regions: Left, the red object is shown with high reflectance at the upper wavelengths. In the middle, due to the shading, this reflectance is decreased. Right, the reflectance of the yellow object is shown, with high reflectance at the upper and middle wavelengths. c: Red plastic object reflecting a strong highlight, while a green plastic object makes up the background.*

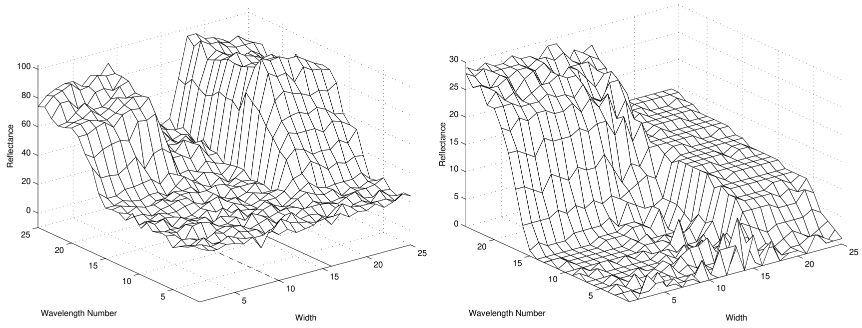

(a) (b)

Figure 2: *a: 3-D graph of the downsampled linescan image of Fig. 1b. The x-axis of the graph represents spatial data, the y-axis the spectral data, and the z-axis the reflectance of the objects. Left, the red object is shown with high reflectance at the upper wavelengths. In the middle, due to the shading, this reflectance is decreased. Right, the reflectance of the yellow object is shown, with high reflectance at the upper and middle wavelengths. b: The normalized spectra of Fig. a is identical for the entire range of the red object. The detected and classified shadow/geometry edges are denoted by the dashed line at the bottom of the graph, the detected and classified material edge is shown as a solid line.*

after which 25 samples are taken in the 450 - 700 nm range. This spectral line scan image thus has a dimension of 760 x 1 x 25. A visually comprehensive representation of the sampled linescan image of Fig. 1b is shown in Fig. 2a where both the spectral and spatial information are downsampled.

In Section 4, a rule-based edge classifier was presented. Based on comparison of the edge maps from raw hyper-spectra and from normalized hyper-spectra, shadow/geometry edges and material edges can be distinghuised. This is demonstrated in Fig. 2b where the normalized spectra are identical for the entire range of the red object. As a result, an edge detector finds the material edge. In contrast, an edge detector operating on the spectrum of Fig. 2a finds the shadow and material edge. The combination of the edge maps thus distinghuishes a shadow/geometry (dashed line at bottom of Fig. 2a) from a material edge (solid line).

The next experiment is conducted on the line-scan obtained from the scene depicted in Fig. 1c. Here, a red plastic object reflects a strong highlight, while a green plastic object makes up the background. The highlight edges are detected by comparison of the normalized spectral and the hue edge map. To compute the hue, the spectra are 'equal-energized' or 'white-balanced'. The resulting spectra are shown in Fig. 3a. Next, the spectra are desaturated, the resulting spectra are shown in Fig. 3b. The experiment shows that the amount of highlight present in Fig. 3b is reduced compared to that of Fig. 3a. Due to noise, some amount of highlight is still present. However, the decrease of saturation is sufficient to distinghuish the red from the green object using hue, while the red object is recognized as a whole. The edge map computed from the normalized spectra contains one material

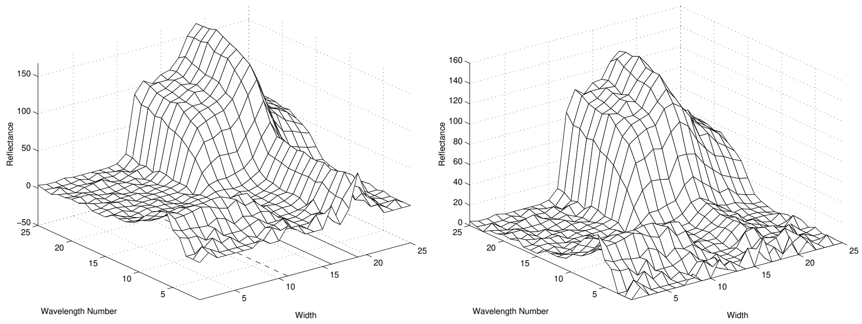

(a) (b)

Figure 3: *a: Plot of line-scan of the region shown in Fig. 1c. The plot can be divided in two regions, the region corresponding to the red object and the region that represents the green object. The highlight is visible in the red region as the subregion with increased reflectance, which is constant over the entire spectral range. b: Desaturated spectra, the amount of highlight is reduced compared to that of a. The detected and classified highlight edges are denoted by the solid line at the bottom of the graph, the detected and classified material edge is shown as a dashed line.*

edge and two highlight edges, while the hue edge map contains only the material edge. The detected and classified highlight edges are denoted by the solid line at the bottom of the graph of Fig. 3a, the detected and classified material edge is shown as a dashed line.

In Fig. 4, the edge classifier operates on edge maps obtained from RGB data. The image is taken with a properly white-balanced Sony XC-003P camera. The image in Fig. 4a shows a number of toys. Highlights and shadows are present in the image. In Fig. 4b, edges classified as material edges are shown in red, edges classified as highlight edges in white, and edges classified as shadow/geometry edges in blue. The experiment shows that the proposed methods for hue calculation and edge classification are also valid for ordinary RGB images.

6 Summary

Methods were presented for hyper-spectral color space transforms and for edge detection in hue images. In theory, the effect of varying imaging conditions was analyzed for raw hyper-spectra, for normalized hyper-spectra, and for hue computed from hyper-spectra. From the theoretical results, an edge classifier was derived which distinghuishes edges from the following types: (1) a shadow or geometry edge, (2) a highlight edge, (3) a material edge. The theoretical results were confirmed by experiments.

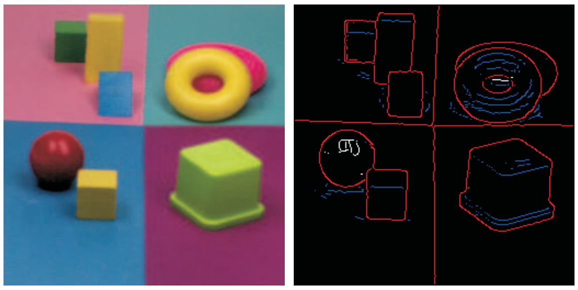

(a) (b)

Figure 4: *a: A number of toys with highlights and shadows. b: Classified edges. Material edges are shown in red, highlight edges in white, and shadow edges in blue. The experiment shows that the proposed methods for hue calculation and edge classification are also valid for conventional RGB images.*

References

[1] R. Bajcsy, S. W. Lee, and A. Leonardis. Color image segmentation with detection of highlights and local illumination induced by inter-reflections. In *IEEE 10th International Conference Pattern Recognition '90*, pages 785–790, Atlantic City, New Jersey, 1990.

[2] J. F. Canny. A computational approach to edge detection. *IEEE Transactions Pattern Analysis and Machine Intelligence*, 8(6):679–698, 1986.

[3] Theo Gevers and Harro Stokman. Reflectance based edge classification. In *Vision Interface '99*, pages 25–32, Trois-Rivieres, Canada, 19-21 May 1999.

[4] G. Healey. Segmenting images using normalized color. *IEEE Transactions on Systems, Man and Cybernetics*, 22(1):64–73, 1992.

[5] Gudrun J. Klinker, Steven A. Shafer, and Takeo Kanade. A physical approach to color image understanding. *International Journal Computer Vision*, pages 7–38, 4 1990.

[6] Steven A. Shafer. Using color to separate reflection components. *Color Research Applications*, 10(4):210–218, Winter 1985.

[7] Silvano Di Zenzo. A note on the gradient of a multi-image. *Computer Vision, Graphics, and Image Processing*, 33:116–125, 1986.